Unusual Magnetic Behaviors and Electronic Configurations Driven by Diverse Co(II) or Mn(II) MOF Architectures

María Celeste Bernini,[†,‡] Julio Romero de Paz,[§] Natalia Snejko,[‡] Regino Sáez-Puche,[§,⊥] Enrique Gutierrez-Puebla,[‡] and María Ángeles Monge*,[‡]

[†]Área de Química General e Inorgánica, Facultad de Química, Bioquímica y Farmacia, Universidad Nacional de San Luis. Instituto de Tecnología Química, INTEQUI-CONICET, San Luis, Argentina

[‡]Instituto de Ciencia de Materiales de Madrid, ICMM, CSIC, Madrid, Spain

[§]C.A.I. Técnicas Físicas, Facultad de Ciencias Físicas, Universidad Complutense de Madrid, Ciudad Universitaria s/n, 28040-Madrid, Spain

S *Supporting Information*

ABSTRACT: Five novel metal organic frameworks were obtained by hydro-solvothermal reactions using the hexafluorisopropylidenebis(benzoic) acid (H_2hfipbb) as linker and Co(II) or Mn(II) ions as connectors. $[Co_2(Hhfipbb)(TEA)]$, compound **1** (TEA = triethanolamine trianion) with a three-dimensional (3D) framework, and a **tpu** net; $[Co_{1.5}(hfipbb)_2]\cdot HN(CH_2CH_3)_3$ and $[Co_3(hfipbb)_2]\cdot 2\{HN(CH_2CH_3)_3\}$, compounds **2** and **2-a**, respectively, both with two-dimensional structure, **sql** topologies, and different layer packings. Compounds **3** and **4**, having the general formula $[M_2(hfipbb)_2]\cdot C_7H_8$, where M = Co (**3**) or Mn (**4**), have 3D frameworks with an **sqc** topology. A deep analysis of the magnetic measurements reveals different striking magnetic behaviors resulting from diverse secondary building unit and framework architectures. Compound **1** presents canted antiferromagnetic chains, compound **2** contains ferromagnetic linear trimeric clusters, and compound **3** exhibits ferromagnetic chains. For the three compounds, a 3D canted antiferromagnetic structure takes place at ∼8 K by means of weak magnetic interactions between the mentioned magnetic units. Such long-range magnetic order is precluded with the application of a high enough magnetic field. Compound **4** evidenced intrachain antiferromagnetic interactions.
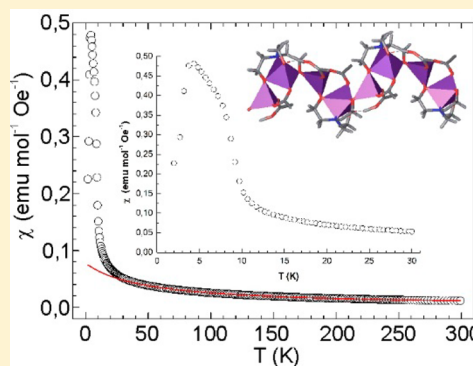
INTRODUCTION

Metal–organic frameworks (MOFs) are a class of materials constructed from the joining of organic linkers with metal ions or clusters.[1] MOFs have great potential for multiple applications depending on their structure, chemical composition, particle size, etc. Thus, in the last decades, MOFs have demonstrated usefulness in fields such as hydrogen and methane storage[2] capture and separation of CO_2,[3] water adsorption,[4] solvent sponge behavior,[5] controlled drug entrapment and release,[6] heterogeneous catalysis,[7,8] luminescence,[9] etc. While many of these applications are based on the framework porosity, yet MOF materials also exhibit physical properties traditionally associated with highly dense oxide systems. For example, MOFs may also have interesting magnetic properties because the magnetic metal ions and their coupling can be tailored[10] in the MOF structure through the incorporation of magnetic moment carriers such as paramagnetic metals, open-shell organic ligands, or both.[11] Paramagnetic transition metal elements allow the variation of spin quantum number and magnetic anisotropy, two important parameters in magnetism. Among these elements, Co(II) appears as a preferred choice to develop magnetic MOFs, because it provides the highest magneto-crystalline anisotropy,

which results in record magnetic hardness. In addition, the coordination environment of Co(II) is adaptable, since it can adopt a wide range of geometries, such as octahedral, tetrahedral, square pyramidal, trigonal-bipyramid, and square-planar, and there are examples of MOFs where this element appears with different coordination polyhedra within the same framework.[12] Moreover, Co(II) cations might appear in the form of clusters, chains, layers, and inorganic three-dimensional (3D) networks, providing a whole gamut of arrangements that are very useful in the understanding of MOF magnetism.[13]

As magnetism is a cooperative phenomenon, a connection between moment carriers at distances within interacting range is necessary; carboxylic-based and nitrogen-based ligands have proved to have good superexchange pathways for magnetic couplings.[13]

In a previous study and working with 3d metal ions (Mn^{2+}, Co^{2+}, Ni^{2+}) and the flexible hexafluoroisopropylidenebis-(benzoic) acid (H_2hfipbb) as linker we have shown that by tuning the MOF synthetic conditions it is possible to obtain

Table 1. Structural and Refinement Details of Compounds 1−4

	compound 1	compound 2	compound 2-a	compound 3	compound 4
formula	$Co_2C_{23}H_{21}F_6NO_7$	$Co_3C_{80}H_{64}F_{24}N_2O_{16}$	$Co_3C_{80}H_{62}F_{24}N_2O_{16}$	$Co_2C_{34}H_{16}F_{12}O_8{}^a$	$Mn_2C_{34}H_{16}F_{12}O_8{}^a$
temperature/K	296(2)	296(2)	296(2)	296(2)	296(2)
radiation λ/Å	Mo Kα = 0.710 73	Cu Kα = 1.541 78	Mo Kα = 0.710 73	Cu Kα = 1.541 78	Cu Kα = 1.541 78
molecular weight/g mol^{-1}	655.27	1942.12	1940.11	898.33	890.35
crystal system	orthorhombic	triclinic	monoclinic	tetragonal	tetragonal
space group	$Pna2(1)$	$P\bar{1}$	$P2(1)/c$	$I4(1)/a$	$I4(1)/a$
a/Å	26.673(7)	12.7610(4)	12.3614(8)	28.3363(3)	28.5047(3)
b/Å	9.769(3)	13.2384(4)	25.6247(17)	28.3363(3)	28.5047(3)
c/Å	10.315(3)	13.7262(5)	13.7747(9)	10.5361(3)	10.5027(3)
α/deg	90	83.886(2)	90	90	90
β/deg	90	89.474(2)	93.4580(10)	90	90
γ/deg	90	66.4220(10)	90	90	90
V/Å^3	2687.6(12)	2111.74(12)	4355.3(5)	8459.9(3)	8533.6(3)
Z	4	1	2	8	8
calc. density/g cm^{-3}	1.619	1.527	1.479	1.411	1.386
μ/mm^{-1}	1.318	5.616	0.679	7.024	5.688
dimensions (mm)	0.18 × 0.06 × 0.02	0.3 × 0.2 × 0.1	0.2 × 0.12 × 0.08	0.4 × 0.08 × 0.06	0.16 × 0.08 × 0.04
limiting indices h	−31 < h < 31	−11 < h < 14	−14 < h < 15	−31 < h < 31	−31 < h < 30
k	−11 < k < 11	−8 < k < 15	−32 < k < 31	−23 < k < 31	−32 < k < 31
l	−12 < l < 12	−15 < l < 15	−17 < l < 17	−3 < l < 11	−11 < l < 10
$F(000)$	1320	983	1962	3568	3536
reflections collected/unique with $I > 2\sigma(I)$	4426/2867	6497/4504	8863/4771	3089/2276	3345/2852
refined parameters	356	574	502	253	253
goodness-of-fit on F^2	1.104	0.935	0.959	1.129	1.124
R_1	0.0856	0.0641	0.0775	0.0495	0.0392
wR_2	0.1209	0.1548	0.2225	0.1637	0.1192
R-factor-all	0.1578	0.0823	0.1496	0.0682	0.0448

^{a}The formulas and molecular weights do not consider the presence of the toluene in the channels.

compounds where the metal ions are at appropriate distances to present ferromagnetism.[14]

Following this study, here we report five new compounds belonging to three novel structural types. These new compounds have been synthesized with the combination of H$_2$hfipbb and Co(II) (compounds 1, 2, 2a, and 3) or Mn(II) (compound 4). The new compounds show interesting magnetic behavior arising from their different inorganic secondary building units (SBUs) and the interactions among them. Thus, compounds 1, 2, and 3 exhibit 3D canted antiferromagnetic structures at ∼8 K. Synthetic aspects and structural and topological analyses along with magnetic properties are discussed in detail in subsequent sections.

■ EXPERIMENTAL SECTION

General Synthesis Procedures. *[Co$_2$(Hhfipbb)(TEA)] (1).* This compound (TEA = triethanolamine trianion) was obtained by hydrothermal reaction of 1 mmol of CoCl$_2$·6H$_2$O with 1 mmol of the ligand (H$_2$hfipbb = C$_{17}$H$_{10}$O$_4$F$_6$) in a mixture of water (5 mL) and triethanolamine (N(CH$_2$CH$_2$OH)$_3$, 1 mL). The mixture was put in a Teflon-lined digestion bomb (internal volume of 43 mL), at 220 °C during 5 h and then cooled to room temperature. Prismatic blue platelike crystals were collected after washing with distilled water and acetone (yield 83.7%). Elemental analysis calcd (%) for [Co$_2$C$_{23}$H$_{21}$F$_6$NO$_7$] C: 42.12, N: 2.14, H: 3.20; found C: 42.19, N: 2.22, 2.93.

[Co$_{1.5}$(hfipbb)$_2$]·HN(CH$_2$CH$_3$)$_3$ (2). This compound was obtained by hydrothermal reaction of 0.6 mmol of CoCl$_2$·6H$_2$O with 0.8 mmol of the ligand (H$_2$hfipbb), in 6 mL of water with 0.2 mL of triethylamine. The mixture was put in Teflon-lined digestion bombs (internal volumes of 43 mL), at 200 °C during 7 d and then cooled to room temperature. Violet single crystals were collected after washing with distilled water and acetone. Elemental analysis calcd (%) for

[Co$_3$C$_{80}$H$_{64}$F$_{24}$N$_2$O$_{16}$] C: 49.43, N: 1.44, H: 3.29; found C: 49.22, N: 1.34, H: 3.32.

If the same reactant mixture, with only 0.1 mL of triethylamine, is heated at 170 °C during 6 d, a mixture of compounds is obtained. Such mixture contains the previously reported compound 3 of ref 14, the current compound 2, and some crystals of another compound with formula [Co$_3$(hfipbb)$_2$]·2{HN(CH$_2$CH$_3$)$_3$}, named 2-a from now on.

[Co$_2$(hfipbb)$_2$]·C$_7$H$_8$ (3) and [Mn$_2$(hfipbb)$_2$]·C$_7$H$_8$ (4). These compounds were obtained by solvothermal reaction of 0.5 mmol of CoCl$_2$·6H$_2$O or MnCl$_2$·4H$_2$O with 0.5 mmol of the ligand (H$_2$hfipbb), in 6 mL of toluene with three drops of triethylamine and five drops of distilled water. The mixtures were put in Teflon-lined digestion bombs (internal volumes of 43 mL), at 180 °C during 4 d and then cooled to room temperature. Light blue platelike single crystals of 3 and colorless platelike single crystals of 4 were collected after washing with acetone. Elemental analysis calcd (%) for [Co$_2$C$_{41}$H$_{24}$F$_{12}$O$_8$] C: 49.68, H: 2.42; found C: 49.05, H: 2.35; and for [Mn$_2$C$_{39.25}$H$_{22}$F$_{12}$O$_8$] C: 49.09, H: 2.42, found C: 48.66, H: 2.31.

Characterization. Full characterization was performed for those compounds that have been obtained as pure phases (1, 2, 3, and 4). The purity of all compounds was confirmed by comparison of the simulated and experimental powder X-ray diffraction (PXRD) patterns (see Figures S1−S3 in Electronic Supporting Information) along with the elemental analysis results.

Elemental Analysis. It was performed in a CNHS PERKIN ELMER 2400 apparatus.

Single-Crystal Structure Determination and Refinement. Appropriate single crystals of compounds 1 and 2-a were mounted on a Bruker SMART CCD diffractometer, which was equipped with a normal focus, 2.4 kW sealed tube X-ray source (Mo Kα radiation = 0.710 73 Å). Data were collected over a hemisphere of the reciprocal space by a combination of three sets of exposures. Each exposure of 10 s covered 0.3° in ω. Single crystals of compounds 2, 3, and 4 were mounted on a Bruker four circle kappa diffractometer equipped with a Cu INCOATEC microsource operated at 30 W power (45 kV, 0.60
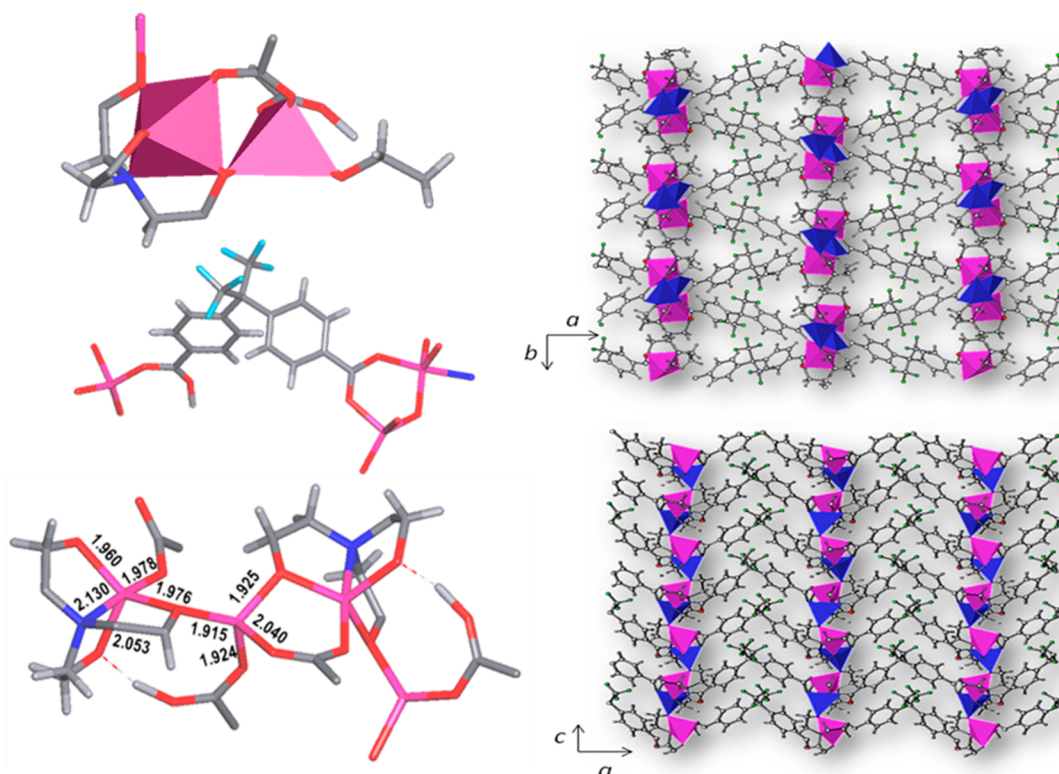
Figure 1. (left) Coordination polyhedra of Co1 and Co2 cations (upper), coordination modes of the Hhfipbb ligand (middle) and details of SBU (lower) of compound **1**. (right) Perspective views of *ab* and *ac* planes of compound **1**.

mA) to generate Cu Kα radiation (λ = 1.541 78 Å), and a Bruker AXIOM area detector (microgap technology). Diffraction data were collected over a hemisphere of reciprocal space in a combination of phi and omega scans to reach a resolution of 0.8 Å (58.91° in θ), using a Bruker APEX2 software suite (each exposure of 10 s covered 0.5° in ω).

Unit cell dimensions were determined by a least-squares fit of reflections with $I > 2s(I)$. The structures were solved by direct methods and refined by anisotropic full-matrix least-squares, except for hydrogen atoms, in the $Pna2_1$ (compound **1**), as $P\bar{1}$ (compound **2**) or $I4_1/a$ (compounds **3** and **4**) space groups. A summary of the conditions for data collection and structure refinement is given in Table 1. All calculations were performed using SMART software for data collection; SAINT plus program[15] for integration and scale correction of data; SHELXTL[16] to solve and refine the structure and to prepare material for publication. In the case of compounds **3** and **4**, once the corresponding structures were solved, a continuous area of electron density was observed all along the main channels. After unsuccessfully trying several disorder models, to model these areas, the electron density was extracted with the Platon Squeeze program.[17]

Powder X-ray Diffraction Data. These measurements were performed with a Bruker D8 diffractometer in the θ−θ mode using nickel-filtered Cu Kα$_{1,2}$ (λ = 0.154 18 nm) radiation. The best counting statistics were achieved by using a scanning step of 0.02° between Bragg angles of 5 and 40° with an exposure time of 2 s per step (see Supporting Information, Figures S1−S3).

Thermogravimetric and Differential Thermal Analyses. These measurements were performed using a SEIKO TG/DTA 320 apparatus in the temperature range of 25−900 °C in air (flow of 100 mL min^{-1}) at a heating rate of 10 °C min^{-1} (see Supporting Information, Figures S4−S7).

Infrared Spectroscopy. The IR spectra were recorded from KBr pellets in the range of 4000−250 cm^{-1} on a PerkinElmer spectrometer (see Supporting Information, Figures S8−S10).

Magnetic Measurements. Magnetization measurements were carried out on polycrystalline samples using a superconducting quantum interference device magnetometer (Quantum Design, model MPMS-XL). The temperature dependence of the molar magnetic susceptibility $\chi(T)$ was obtained from the direct current (dc) magnetization (M) measured with an applied magnetic field (H) during warming the sample from 2 to 300 K. Zero-field cooling and field cooling measurement modes were used. In the former, the sample was cooled from room temperature to 2 K in zero field, and in the latter the sample was cooled in the measuring H. The magnetic field dependence of the dc magnetization $M(H)$ was obtained at different temperatures up to ±5 T. The temperature dependence of the real and imaginary part of the alternating current (ac) molar magnetic susceptibility, $\chi'_{ac}(T)$ and $\chi''_{ac}(T)$, respectively, was obtained from the ac magnetization measured in the temperature range of 2−35 K, with $H = 0$ and applying an oscillating magnetic field with drive amplitude of 0.35 mT at different frequencies in the range of 1−1000 Hz. The diamagnetic contribution[18] was subtracted from the calculated molar susceptibilities χ.

■ RESULTS AND DISCUSSION

Synthesis. To achieve different framework architectures, in which the metal condensation and intermetallic distances allow magnetic interactions, diverse synthetic approaches were explored as follows.

We chose TEA as a coligand in the synthesis of compound **1** because: (i) it is a small molecule with several donor atoms in close positions that help in the metal ion condensation by means of bridging bonds; (ii) its coordination ability have been demonstrated in several polynuclear TM complexes;[19] and (iii) it has an additional feature of regulate the pH accepting protons by its nitrogen atoms. In **2** and **2-a** compound syntheses, the triethylamine molecule was employed on the base of our previous results, which verified that by changing the content of this base along with a fine-tune of synthesis temperature, different structures with magnetic order[14] can be achieved.

Solvents polarity and molecular bulkiness were also taken into account, since they play an important role in the rational design and preparation of desired systems.[20] In this sense, the use of nonpolar (aprotic) solvents has been less studied in the MOFs synthesis. However, we have previously studied the use of benzene as a cosolvent with water, in the synthesis of a Ho-succinate framework, where template and structure directing agent (SDA) roles have been exhibited by the aromatic molecule depending on the added content.[21]

In this context, and knowing that toluene has one of the lowest dielectric constant and one of the highest van der Waals volumes, we also explored the use of this aprotic molecule as solvent in the synthesis of compounds **3** and **4**.

Structural Description. *[Co₂(Hhfipbb)(TEA)] (1).* This compound crystallizes in the orthorhombic $Pna2_1$ space group. In the asymmetric unit there are two crystallographic nonequivalent Co(II) ions, one partially deprotonated (Hhfipbb) linker, and one completely deprotonated triethanol-amine molecule. Co1 ion is pentacoordinated to the four TEA donor atoms (one N and three O atoms) and to one O atom from the Hhfipbb deprotonated carboxylate, in a distorted triangular bipyramid. Co2 ion is surrounded by four oxygen atom in a rather tetrahedral geometry, two coming from the TEA anion and the other two coming from two carboxylate groups of different Hhfipbb linkers. As a result, the linker bonds Co1 and Co2 atoms through an $\eta_2\mu_2$ bidentate-bridge mode and bonds the other Co2 (symmetrically related) ion in an η_1 monodentate mode through the protonated carboxylate oxygen (see Figure 1). A very strong H-bond interaction is identified between the protonated carboxylic group and one oxygen atom of the TEA ligand, which is reflected in quite similar donor–hydrogen and hydrogen-acceptor bond distances, being O–H = 1.221 Å and H···O = 1.395 Å. An analogous situation with one hydrogen atom located between two oxygen atoms resulting in similar bond distances was also observed for a Mn-MOF based on the same ligand.[14]

The TEA oxygen atoms are linked to the Co1 ion, in a triple-chelating scorpionate manner, but two of them are also bridging two neighbors Co2 ions (see Figure 1). In this way, each TEA ligand connects three adjacent Co cations to render inorganic sharing vertex polyhedral chains that run in zigzag along the *c* direction (see Figure 1, right). The Co1–O3–Co2 angle is ∼109.6°, and the Co1···Co2 distance is ∼3.17 Å, while the Co2–O5–Co1 angle is ∼116.4° and the Co2···Co1 distance is ∼3.31 Å (see Supporting Information, Figure S11).

In this way, the TEA ligand is the responsible for the condensation of the metal ions to form rod-shaped SBUs and the Hhfipbb one acts as linker connecting the chains to give the 3D net. As can be seen in Figure 1, right, the Hhfipbb linker are displayed in the *ac* plane in a parallel way, thus giving B-type channels,[22] which are fully occupied by the coordinated TEA molecule. The most relevant geometric features of the Hhfipbb linker was also studied, since the framework trends can be predicted or explained better by considering them (see Scheme 1).

[Co₁.₅(hfipbb)₂]·{HN(CH₂CH₃)₃} (2). This crystallizes in the $P\bar{1}$ triclinic space group. There are two nonequivalent Co(II) ions. One of them (Co1) located on the on the Wyckoff position 1g, it is coordinated to six oxygen atoms disposed in a quite regular octahedral polyhedron (Co1–O bond distances in the range 2.073–2.098 Å). The other ion (Co2) is surrounded by five oxygen atoms forming a mono capped tetrahedron with four Co2–O bonds in the 1.990–2.087 Å range, and

Scheme 1. Definition of d Distance (left) and ϕ Angle (right)[a]

d_{L1} = 9.43 Å d_{L1-2a} = 9.604 Å
d_{L1-2} = 9.60 Å d_{L2-2a} = 9.94 Å
d_{L2-2} = 9.55 Å d_{L1-2b}* = 10.02 Å
d_{L1-3} = 8.66 Å d_{L2-2b}* = 10.02 Å

ω_{L1-1} = 109.9°
ω_{L1-2} = 68.81°
ω_{L2-2} = 71.88°
ω_{L1-2a} = 74.85°
ω_{L2-2a} = 65.53°
ω_{L1-2b}* = 71.28°
ω_{L2-2b}* = 71.33°
ω_{L1-3} = 71.14°
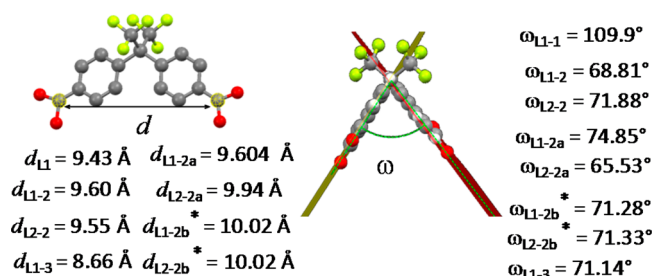
[a]* Compound **2-b** corresponds to compound 2 in reference 34.

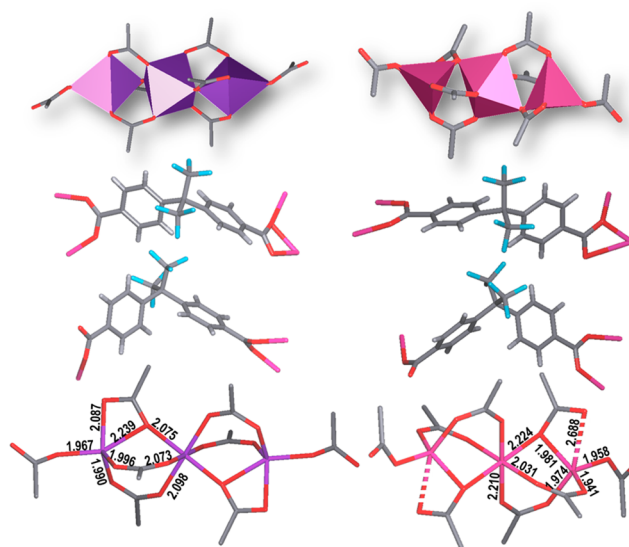complemented with an additional longer Co2–O bond of 2.239 Å (see Figure 2, left). The asymmetric unit also

Figure 2. Coordination polyhedra of Co1 and Co2 cations (upper), coordination modes of the Hhfipbb ligand (middle), and details of SBUs (lower) of compounds **2** (left) and **2-a** (right).

comprises two independent and completely deprotonated hfipbb ligands and one noncoordinated protonated triethyl-amine molecule. Trimeric CoO₅–CoO₆–CoO₅ SBUs are formed via Co(1) octahedron symmetry center. Similar trimeric clusters were also identified in previously reported Mn-hfipbb and Co-hfipbb MOFs obtained using different organic amines as templates.[23] As can be deduced from the charge balance, the framework is anionic having a (−1) charge, and the electroneutrality is achieved by the incorporation of the protonated amine in the voids of the net.

As to the hfipbb anions, one of them acts as $\eta_3\mu_2$–$n_2\mu_2$ tetratopic linker connecting two Co ions in a chelate-bridge mode by one carboxylate group and in a bidentate-bridge mode by the other one. The other ligand is a $\eta_2\mu_2$–η_1 tritopic linker, since joins two Co ions of a trimeric SBU through a bidentate bridge mode, and one Co ion of a different SBU in a mododentate mode (see Figure 2, left). The resulting two-dimensional (2D) framework is formed by layers packed along the *c* direction through Coulombic interactions with the triethylammonium cations (see Figure 3).

[Co₃(hfipbb)₂]·2{HN(CH₂CH₃)₃} (2-a). This compound is a polymorph of compound **2**, with almost identical structure,
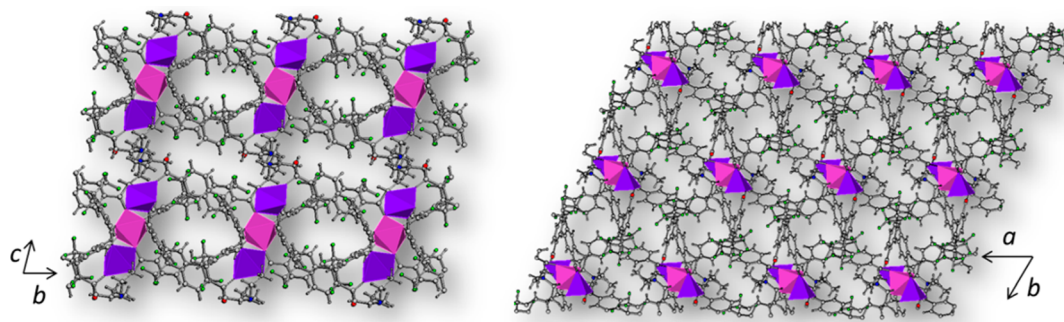
Figure 3. Perspective views of *cb* and *ab* planes of compound **2**.
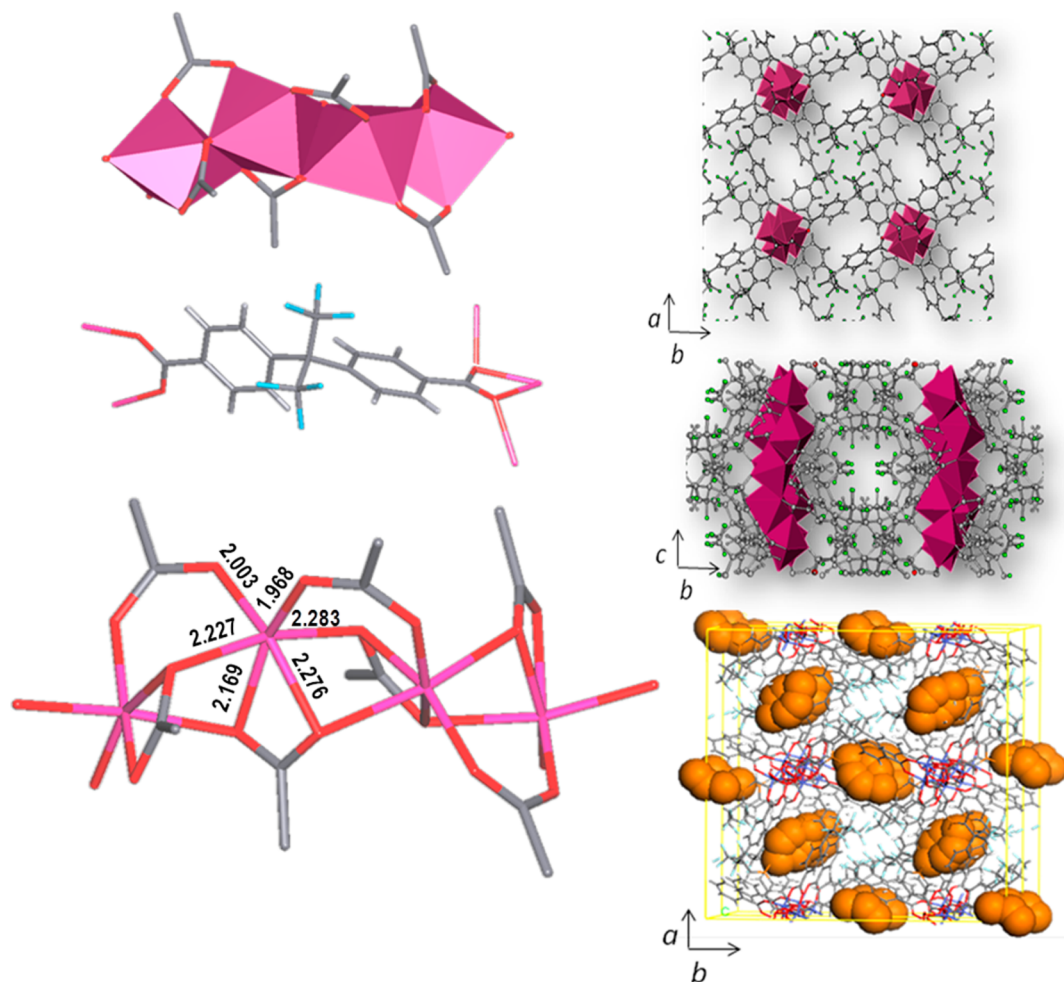

Figure 4. (left) Coordination polyhedra of Co cations (upper), coordination modes of the hfipbb ligand (middle), and details of the SBU (lower) of compound **3**. (right) Perspective views of *ab* (with and without toluene in channels) and *ac* planes of compound **3**.

though it crystallizes in the $P2_1/c$ space group, and it also is isomorphic with a reported[23] Co-hfipbb MOF obtained with dibutylamine instead of triethylamine. Because of this, only the specific geometrical features are now displayed in Figure 2-right and Scheme 1 for comparative purposes.

As was stated above, two quite similar Co-hfipbb layered frameworks have been previously reported having also trimeric clusters.[23] One of those belongs to the $P2_1/c$ space group (referred as compound **2-a*** from now on) and is isomorphous with **2-a** compound, while the other one, belongs to the $C2/c$ space group (named **2-b** from now on). In this way results interesting to analyze the structural resemblances and differ-

ences between **2-a*** and **2-b** with the novel compounds **2** and **2-a**.

Compounds **2** and **2-a** were obtained by using the same organic amine (triethylamine) but using different synthesis temperature (**2** at 200 °C, **2-a** at 170 °C), while the **2-a*** was obtained using 4,4′-trimethylenedipiperidine, being the synthesis temperature 160 °C. Regarding compounds **2-a** and **2-a***, which exhibit an isomorphic character, the occupied volumes of triethylamine and 4,4′-trimethylenedipiperidine molecules have been calculated by means of the accessible solvent surfaces algorithm implemented in the Atom Volumes & Surfaces tool of Materials Studio software,[24] being 291.6 and
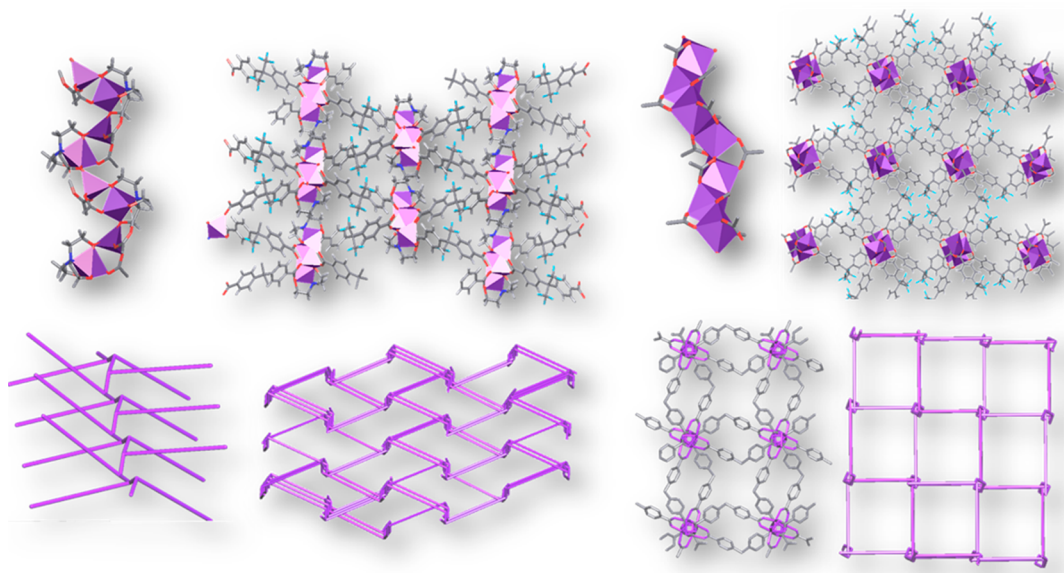
Figure 5. Perspective views, details of the SBUs, and topological representations of compounds **1** (left), **3**, and **4** (right).

734.5 Å^3, respectively. The influence of using a bigger SDA as 4,4′-trimethylenedipiperidine in comparison with using triethylamine is not evidenced neither in the cell volumes (being almost equal) nor in the resultant framework void volumes, whose values were 1208.4 Å^3 (**2-a***) and 1351.7 Å^3 (**2-a**), respectively, representing ∼28% and 31% of the cell volumes, respectively (calculations performed with Platon program[17]). On the contrary, the influence of the 4,4′-trimethylenedipiperidine is evidenced in the higher framework density (1.514 g/cm^3) of **2-a*** in comparison with the corresponding density of compound **2-a** (1.479 g/cm^3). These facts suggests that the bigger amine, containing two donor nitrogen atoms disposed in opposite sides of the molecule allow for exhibiting stronger interactions, driving to a denser isomorphic compound.

Compound **2-b** was synthesized at 180 °C by using dibuthylamine as SDA.

On the basis of this analysis, we can infer that the different amines used in the syntheses of **2**, **2-a**, **2-a***, and **2-b** act not only to regulate the pH but also are driving the framework development leading to similar layered frameworks. Moreover, all of these compounds contains linear trimeric clusters composed by central CoO$_6$ units forming quite regular octahedrons and terminal CoO$_4$ units having one (**2**, **2-a**, and **2-a***) or two (**2-b**) additional longer Co—O bonds. The differences in the terminal CoO$_x$ polyhedra can be associated with different orientations of the carboxylate groups in relation with the aromatic rings. Such differences along with the different geometric features displayed by the hfipbb ligands (see Scheme 1) give rise to the crystallization of very similar structures in different space groups.

[Co$_2$(hfipbb)$_2$]·C$_7$H$_8$ (3) and [Mn$_2$(hfipbb)$_2$]·C$_7$H$_8$ (4). These compounds are isostructural and crystallize in the tetragonal *I*4$_1$/*a* space group. In the following, the structure of compound **3** will be discussed in detail, and the corresponding information to compound **4** will be given in parentheses when necessary. The asymmetric unit contains one crystallographically nonequivalent Co(II) ion and one deprotonated hfipbb ligand.

M (M = Co and Mn) ions are coordinated to six oxygen atoms disposed in a noncentrosymmetric octahedron, with M—O distances in the ranges of 1.968−2.283 Å and 2.0289(16)−

2.3951(15) for Co and Mn, respectively. The hfipbb ligand acts as a penta-topic linker in a $\eta_2\mu_3$ (bidentate-chelate-bis bridge)-$\eta_2\mu_2$ (bidentate-bridge) mode giving rise to infinite edge-sharing zigzag chains of octahedral units that run along the [0 0 1] direction (see Figure 4). These chains are reminiscent of those reported for Ga ion in MIL-120.[25]

These one-dimensional (1D) SBUs are in a square arrangement, and connected among them through the complete organic linker in a 3D framework (see Figure 4). One-dimensional channels, filled with disordered toluene guest molecules, run parallel to the inorganic SBUs. As usually happens with this kind of nonpolar aprotic solvent, without possibility of exhibiting specific interactions inside the framework voids, these molecules are highly disordered. The 1D channels own a potentially available volume of 2636.8 Å^3 per unit cell, which represents 31.2% of the cell volume (according to Platon calculations[17]).

Topological Analysis. Topological analyses of compounds **1**−**4** and of compound **2-a** were performed by using TOPOS program.[26] The structure of compound **1** can be simplified considering the hfipbb ligands as linkers connecting Co1 by one carboxylate group and Co2 by the other one. Each cobalt ion has two additional bonds to the bridging oxygen atoms of the TEA composed by three-connected nodes located on the metallic centers (see Figure 5, left). Such representation is consistent with a **tpu**-type topology, which is a subnet of the **dia** net, and has been associated with noncentrosymmetric coordination polymers exhibiting ferroelectricity and nonlinear optical properties.[27]

The structures of compounds **3** and **4** can be topologically described as uninodal nets, with three-connected nodes located at the centroid positions of the inorganic SBUs. From such centroids, three connections are determined by the carboxylate groups of the ligand. Two connections are along the SBU direction, and the other one is rotating according to the movement of the 4$_1$ screw axis located on the inorganic chains. This gives an **sqc** topological type (see Figure 5, right).

As compounds **2** and **2-a** are both 2D MOFs with linear trimeric SBUs, the cluster simplification methodology was performed on these structures, giving as a result the same
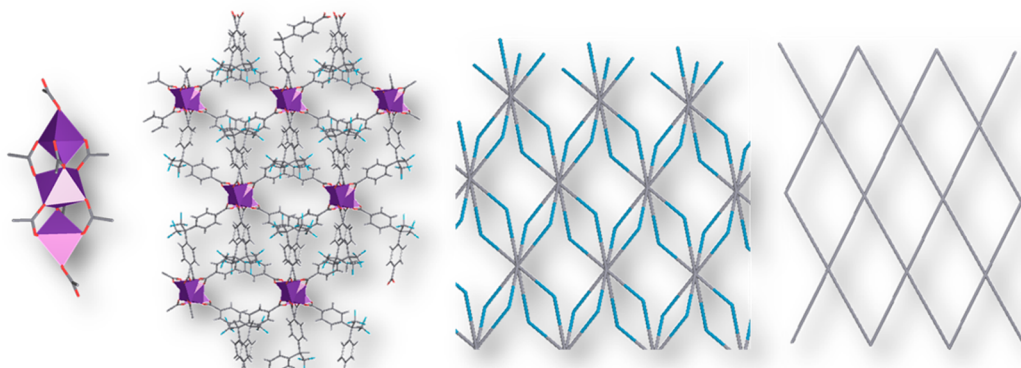
Figure 6. Perspective views and topological representations of compounds **2** and **2-a** (amine cations are omitted for clarity).

uninodal four-connected net corresponding to the **sql/** Shubnikov tetragonal plane type (see Figure 6).

Magnetic Measurements. *Compound 1.* The analysis of $\chi(T)$ for compound **1**, see Figure 7, reveals that this compound
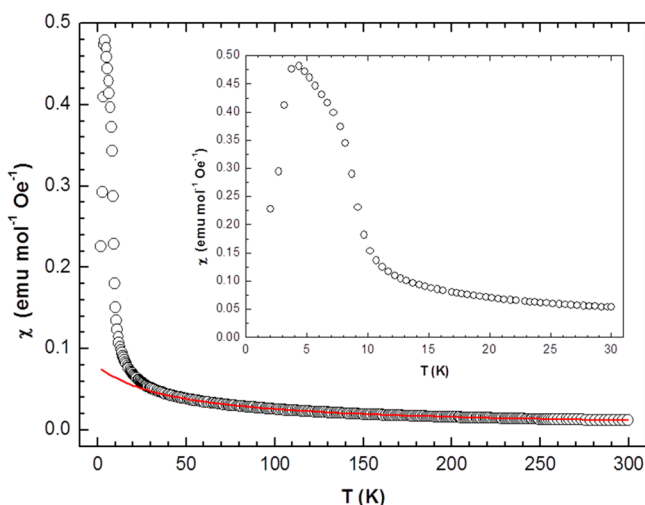

Figure 7. Thermal variation of molar magnetic susceptibility for compound **1** obtained with an applied magnetic field of 100 mT. The solid red line corresponds to the best fit (R^2: 0.999 94) obtained between 50 and 300 K using the function $\chi = (C)/(T - \theta) + TIP$. (inset) The low-temperature region.

shows paramagnetism above ~40 K, following the Curie−Weiss law $\chi = (C)/(T - \theta)$ together with a temperature-independent paramagnetism (TIP) contribution. The best fit of the $\chi(T)$ data between 50 and 300 K to the function $\chi = (C)/(T - \theta) + TIP$ yields $C = 3.50 \pm 0.02$ emu K mol^{-1} Oe^{-1}, $\theta = -44.6 \pm 0.6$ K and TIP = $1.37 \times 10^{-3} \pm 0.04 \times 10^{-3}$ emu K mol^{-1} Oe^{-1}. The experimental χT value at room temperature 3.48 emu K mol^{-1} Oe^{-1} ($\mu_{eff} = 2.828(\chi T)^{1/2} = 5.28$ μ_B per formula unit), a value slightly lower than the expected one for the spin-only case of two high-spin Co^{2+} ions, 3.74 emu K mol^{-1} Oe^{-1}.[28] This could be due to the stabilization of a low-spin ground state for one of the two Co^{2+} ions ($S = 1/2$, expected range of 1.7–2 μ_B per mole of Co^{2+}),[29] but examples of this unusual configuration at room temperature are very scarce.[30] Although the structural data reveal a rather distorted tetrahedral geometry as coordination polyhedron for Co2 atom, it seems more reasonable to explain such a low χT value through moderate short-range antiferromagnetic interactions between the tetrahe-

dral and trigonal bipyramidal Co^{2+} ions. In fact, antiferromagnetic interactions, denoted by the Weiss temperature value (−44.6 ± 0.6 K), are manifested at low temperature for compound **1** as set out below. Upon cooling from 50 K, the $\chi(T)$ curve starts deviating upward from the mentioned Curie−Weiss law just below 40 K (see Figure 7), in spite of the negative value found for θ. Such deviation becomes more noticeable with decreasing temperature until $\chi(T)$ curve shows a sudden increase, which onset is clearly determined in the corresponding χT versus T plot (shown in Supporting Information, Figure S12) by the local minimum centered at 13.5 K. Then, the $\chi(T)$ curve shows a restraint at 8 K on the above-mentioned increase of $\chi(T)$, see inset of Figure 7. This is even more clearly manifested through the sharp maximum reached by χT at 8 K (see Supporting Information, Figure S12) before decreasing to 0.448 emu K mol^{-1} Oe^{-1} at 2 K. Finally, the $\chi(T)$ curve reaches a maximum at 4 K.

The rise of χT at 13.5 K corresponds to the appearance of ferromagnetic-like interactions, confirmed through the non-linear $M(H)$ obtained at 9.5 K (see Supporting Information, Figure S13). Short-range magnetic interactions seem to be their origin because there is no absorption of $\chi''_{ac}(T)$ in the 9−13 K region (see Supporting Information, Figure S14), and no magnetic hysteresis loop is observed at 9.5 K, see Figure 8.
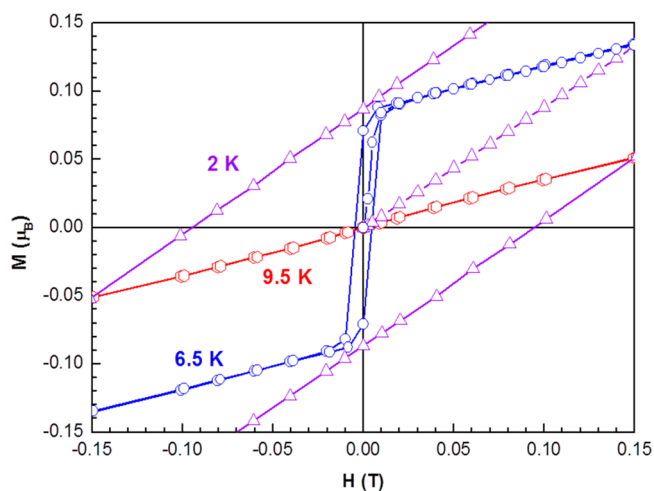

Figure 8. Low magnetic field region of the initial magnetization and the hysteresis loop of compound **1** measured at 2 K (triangles), 6.5 K (circles) and 9.5 K (hexagons). The solid lines are eye guides.

Therefore, such an increase of χT should be originated from the magnetic interactions between neighboring Co^{2+} ions located in the helical chain running along c direction of the crystal structure. From a magnetic point of view this SBU is rather complex due to the alternation of both types of Co^{2+} magnetic centers and two kind of linkages between them, see Figure 1, left and Supporting Information, Figure S11. Thus, there are two effective intrachain superexchange pathways, Co(1)–O(3)–Co(2) and Co(2)–O(5)–Co(1), involving an alcoxo bridge with superexchange angle values of 116.25° and 109.49°, respectively. In the last pathway there is a *syn–syn* carboxylate bridge together with the alcoxo one that could give rise to the so-called counter complementary effect.[31] Such effect will diminish the antiferromagnetic interaction or even turn the sign of the interaction over. In accordance with these values greater than 97° and the negative value of θ, we may state the existence of intrachain antiferromagnetic interactions between the two types of cobalt atoms.[32,33] Therefore, there will be two magnetic phenomena that account for the observed rise of χT, namely, weak ferromagnetism and ferrimagnetism. The rather abrupt rise of χT below 10 K supports the former as the main phenomenon. Concerning the magnetic transition observed at 8 K in Supporting Information, Figure S12, note that $\chi'_{ac}(T)$ curve (Supporting Information, Figure S14) displays also a sharp maximum at the same temperature, which is not shifted varying the measuring frequency, while $\chi''_{ac}(T)$ curve increases. This indicates that a 3D canted antiferromagnetic structure takes place at 8 K through the likely ordering of the canted antiferromagnetic chains. Such nature of this magnetic transition is proved from the $M(H)$ obtained at 6.5 K, since the initial M rapidly increases at very low H values; then it linearly increases to 600 mT (see Supporting Information, Figure S13), and magnetic hysteresis loop is observed (see Figure 8).

This long-range magnetic ordering is rather surprising due to the large distances (see Figure 1, right) between neighbor chains along a and b axis of the structure. Thus, the closest distance between cobalt ions along the a axis, and therefore bridged by the Hhfipbb ligands, is 13.816 Å; and along the b axis, with no ligand, is 7.736 Å. Consequently, the magnetic interactions responsible for the long-range magnetic order of the SBUs are expected to be weak. In this sense, an applied magnetic field of 600 mT at 6.5 K seems to revert the canted antiferromagnetic chains to their noninteracting state judging by both the nonlinear $M(H)$ curve above that critical field and the M value at 5 T ($\sim$1.1 μ_B), see Figure S13.

The maximum found at 4 K, Figure 7, shows all the features of the well-known Hopkinson effect,[34,35] as H increases the maximum grows wider and moves toward lower temperatures and disappears when the sample is cooled in a magnetic field, see Supporting Information, Figure S15.

Finally, to mention that the $M(H)$ observed at 2 K is different from the just mentioned one observed at 6.5 K, seeing that the initial M shows a slow increase at low magnetic fields as H increases (see Figure 8) and therefore the initial M values obtained at 6.5 K are greater than those obtained at 2 K. The cross of both isotherms at 150 mT agrees with the maximum found at 4 K in the $\chi(T)$ curve obtained at 100 mT. Furthermore, the field induced blocking of the interchain interactions observed above 600 mT at 6.5 K seems to be a continuous process at 2 K because it is not possible to identify a critical field at which the changeover takes place. This different behavior becomes strongly apparent when the hysteresis loops

obtained at such temperatures are compared, see Figure 8. Thus, there is a rather important increase of coercivity decreasing temperature, from $\sim$4.5 mT at 6.5 K to $\sim$95 mT at 2 K. Neither the $\chi(T)$ data—or the corresponding $\chi T(T)$—nor the $\chi_{ac}(T)$ data reveal any magnetic transition that accounts for such differences. Therefore, the difference in the shapes of the $M(H)$ curves may arise from the temperature dependence of the domain structure of the material.

Compound 2. The analysis of $\chi(T)$ for compound **2** (see Supporting Information, Figure S16) reveals that this compound shows paramagnetism above $\sim$30 K. The best fit of the $\chi(T)$ data between 50 and 300 K to the function $\chi = (C)/(T - \theta) + $ TIP yields $C = 8.814 \pm 0.005$ emu K mol^{-1} Oe^{-1}, $\theta = -8.64 \pm 0.06$ K, and the TIP term can be neglected. The χT value at room temperature is 8.57 emu K mol^{-1} Oe^{-1} ($\mu_{eff} = 2.828(\chi T)^{1/2} = 8.29$ μ_B per formula unit), a value consistent with the presence of three high spin Co^{2+} ions. Below 30 K the $\chi(T)$ curve starts deviating upward from the mentioned Curie–Weiss law, and χ^{-1} tends toward zero, in the same way that the magnetic susceptibility of noninteracting octahedral Co^{2+}.[28] However, the $\chi_{ac}(T)$ obtained at low temperature with $H = 0$ reveals a rather complex behavior, see Figure 9. Thus, as temperature decreases $\chi_{ac}T$ decreases to
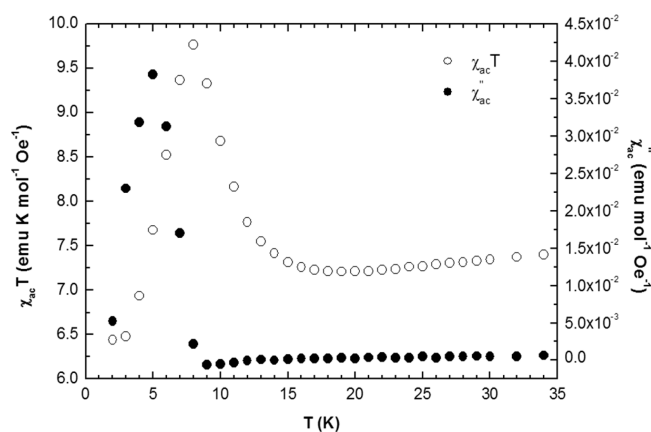

Figure 9. Thermal variation of the product $\chi_{ac}T$ ($\bigcirc$) and the imaginary part of ac molar magnetic susceptibility ($\bullet$) for compound **2** obtained in the absence of an external magnetic field, applying a drive amplitude of 0.35 mT at 20 Hz.

reach a local minimum at 19 K, and then it shows an increase reaching the maximum value at 8 K before dropping sharply down to the lowest temperature. This maximum is accompanied by an absorption in χ''_{ac} that does not show frequency dependence. Such a minimum indicates the appearance of ferromagnetic-like interactions, which likely take place within the linear trimeric clusters. The slight nonlinear $M(H)$ curve obtained at 14 K and their M value at 5 T ($\sim$3.8 μ_B), see Supporting Information, Figure S17, confirm this point. In the trimeric cluster (see Figure 2-left) the adjacent cobalt atoms (separated by 3.512 Å) are connected by two carboxylate groups, that is Co–O–C–O–Co supersuperexchange pathways, and one bridging oxygen atom of a third carboxylate. The two carboxylate bridges bring weak antiferromagnetic exchange interactions and in the case of the oxygen bridge the exchange interaction is assumed antiferromagnetic according to the value of the Co–O–Co angle, 108.9°. Therefore, in order to account for the observed net magnetization in compound **2** an orbital counter complementary effect[33] must be invoked bringing

along a ferromagnetic interaction in view of the small Co−O− Co angle.

Finally, the observed magnetic behavior below 8 K can be justified considering the onset of long-range antiferromagnetic interactions between ferromagnetic clusters together with a canting of the ordered magnetic moments. It is worthy of note that this magnetic behavior below 8 K is not observed with $H = 100$ mT, which seems to be a high enough magnetic field to preclude the very weak long-range magnetic interactions between the cobalt clusters given the large distances (see Figure 3) between them along the a and b axis of the structure (12.077 and 13.052 Å, respectively, as the shortest distances between cobalt ions bridged by hfipbb ligands). This picture is congruent with the magnetization value of 6.0 μ_B obtained at 5 T and 5 K (see Supporting Information, Figure S17), which is consistent with three Co^{2+} ions with an effective spin $S = 1/2$ and an isotropic g value of about 4.[37]

Compound 3. The $\chi(T)$ obtained for compound 3 follows the function $\chi = (C)/(T - \theta)$ + TIP between 100 and 300 K, and the best fit of the $\chi(T)$ data to that function yields $C = 7.01 \pm 0.02$ emu K mol^{-1} Oe^{-1}, $\theta = 1.1 \pm 0.2$ K, and TIP $= 2.1 \times 10^{-4} \pm 0.4 \times 10^{-4}$ emu mol^{-1} Oe^{-1}. The χT value at room temperature calculated ignoring the TIP is 7.04 emu K mol^{-1} Oe^{-1} ($\mu_{eff} = 2.828(\chi T)^{1/2} = 7.50$ μ_B per formula unit), a value consistent with the presence of two high-spin Co^{2+} ions. The positive value of θ denotes likely ferromagnetic interactions between cobalt atoms (separated by 3.214 Å) as one might expect according to the chains of edge-sharing CoO$_6$ octahedra present in this compound (see Figure 4, left), given that Co− O−Co angles of less than 97° (92.15 and 90.87°) promote ferromagnetic exchange interaction in the case of Co^{2+}.[33,34] It is indeed what the $\chi(T)$ data at low temperature suggest, showing a similar magnetic behavior to that one proposed above for compound 1. This is hardly surprising because both compounds have as SBUs magnetic chains of cobalt polyhedra connected through the almost same ligand. Thus, the χT versus T plot shown in Figure 10 reveals a minimum centered at 26 K corresponding to the onset of intrachain ferromagnetic interactions. The sharp maximum at 7 K corresponds to antiferromagnetic interactions between the ferromagnetic chains. Furthermore, the absorption of $\chi''_{ac}(T)$ (see Supporting Information, Figure S18) reveals the development of weak

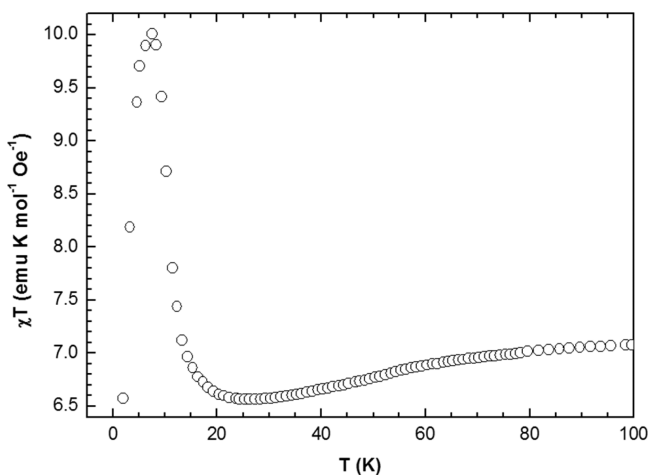ferromagnetism. Finally, the $M(H)$ data obtained at 2 K (see Supporting Information, Figure S19) show a value of 2.75 μ_B at 5 T, which can be justified by the presence of noninteracting ferromagnetic chains due to the effect of the applied magnetic field.

Compound 4. The $\chi(T)$ obtained for compound 4, see Figure 11, follows a Curie−Weiss law $\chi = (C)/(T - \theta)$
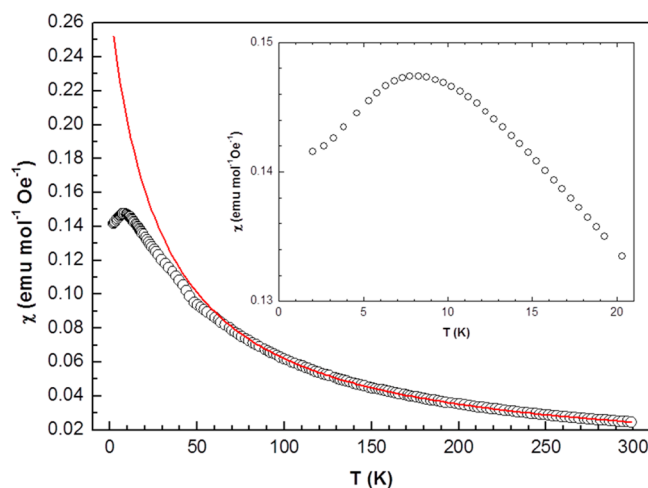

Figure 11. Thermal variation of molar magnetic susceptibility for compound 4 obtained with an applied magnetic field of 100 mT. The solid red line corresponds to the best fit ($r^2 = 0.999\,98$) obtained between 100 and 300 K using the function $\chi = (C)/(T - \theta)$. (inset) The low-temperature region.

between 100 and 300 K and the best fit of the $\chi(T)$ data to that function yields $C = 8.067 \pm 0.005$ emu K mol^{-1} Oe^{-1} and $\theta = -29.8 \pm 0.1$ K. The χT value at room temperature is consistent with the presence of two Mn^{2+} ions ($S = 5/2$). Below 80 K $\chi(T)$ curve starts deviating downward from the mentioned Curie−Weiss and such deviation becomes more noticeable with decreasing temperature. However, there is an increase of $\chi(T)$ curve at 47 K that is likely due to the presence of a small amount of ferrimagnetic Mn$_3$O$_4$[36] oxide as an impurity. At lower temperature, it is observed a well-defined maximum at 8 K.

This behavior points out the action of antiferromagnetic interactions between Mn^{2+} ions in accordance with the negative value found for θ. These manganese atoms are located in chains of edge-sharing MnO$_6$ octahedra (see Figue 4, left) with a nearest-neighbor distance of 3.286 Å and Mn−O−Mn angles of 90.080 and 93.042°. We tried the $\chi(T)$ data fit to several expressions to estimate the value of intra- and interchain exchange coupling constants, but the goodness of the fits precluded their inclusion in this work. The certain reason for this is the presence of the Mn$_3$O$_4$ impurity. However, taking into account the fact that the closest distance between manganese ions in different chains and bridged by the hfipbb ligand is 12.764 Å (see Figure 4, right), the maximum centered at 8 K could mainly correspond to intrachain antiferromagnetic interactions due to the expected weakness of the interchain magnetic interactions.

Figure 10. Thermal variation of the product χT corresponding to the molar magnetic susceptibility measured in an applied field of 100 mT for compound 3.

■ CONCLUSIONS

Five novel MOFs based on Co(II) or Mn(II) and the hexafluorisopropylidenebis(benzoic) acid, belonging to four structural types, have been obtained as pure phases, by hydro-

solvothermal synthesis. The role of triethanolamine as coligand bridging cobalt ions in the SBU of compound **1**, triethylamine as an SDA of **2** and **2-a**; and toluene as a template of compounds **3** and **4** was verified. A wide diversity of coordination geometries and framework dimensionality was evidenced in the present structures, standing out the strong versatility of the flexible hfipbb ligand for framework developments. Helical 1D chains formed by corner-sharing alternating CoO_4 and CoO_5 polyhedra in **1**, trimeric clusters of $CoO_5-CoO_6-CoO_5$ in **2** and **2-a**, and edge-sharing 1D chains of CoO_6 or MnO_6 polyhedra in **3** and **4**, were identified as SBUs in the novel structures. Compound **1**, belonging to the polar *mm*2 point group has a quite rare **tpu** topology, while **2** and **2-a** can be described as **sql** plane nets, exhibiting different layer packings. Compounds **3** and **4**, being isostructural, resulted in **sqc** topological type. The compounds based on Co(II) show a rather complex magnetic behavior at low temperature. Compounds, **1**, **2**, and **3** show low-dimensional magnetic interactions manifested through the appearance of an abrupt rise of χT, whose origin depends on the SBU constitution. Thus, compound **1** presents canted antiferromagnetic chains, compound **2** presents ferromagnetic linear trimeric clusters, and compound **3** ferromagnetic chains. For the three compounds, a 3D canted antiferromagnetic structure takes place at ∼8 K by means of weak magnetic interactions between the mentioned magnetic units. Such long-range magnetic order is precluded with the application of a high enough magnetic field.

ASSOCIATED CONTENT

Ⓢ Supporting Information

Crystallographic information files (cifs), simulated and experimental PXRD patterns, TG-DTA curves, FTIR spectra, structural details for compound **1**, and complementary magnetic measurements. This material is available free of charge via the Internet at http://pubs.acs.org. CCDC reference numbers 1017406−1017410 contain the supplementary crystallographic data for this paper. These data can be obtained free of charge from the Cambridge Crystallographic Data Centre via www.ccdc.cam.ac.uk/data_request/cif.

AUTHOR INFORMATION

Corresponding Author

*E-mail: amonge@icmm.csic.es. Fax: +34913720623.

Present Address

⊥Departamento de Química Inorgánica, Facultad de Ciencias Químicas, Universidad Complutense de Madrid, Ciudad Universitaria s/n, 28040-Madrid Spain.

Notes

The authors declare no competing financial interest.

ACKNOWLEDGMENTS

REFERENCES

(1) Furukawa, H.; Cordova, K.; O'Keeffe, M.; Yaghi, O. *Science* **2013**, *341*, 974.

(2) Gándara, F.; Furukawa, H.; Lee, S.; Yaghi, O. M. *J. Am. Chem. Soc.* **2014**, *136*, 5271.

(3) Fracaroli, A. M.; Furukawa, H.; Suzuki, M.; Dodd, M.; Okajima, S.; Gándara, F.; Reimer, J. A.; Yaghi, O. M. *J. Am. Chem. Soc.* **2014**, *136*, 8863−8866.

(4) Furukawa, H.; Gándara, F.; Zhang, Y.-B.; Jiang, J.; Queen, W. L.; Hudson, M. R.; Yaghi, O. M. *J. Am. Chem. Soc.* **2014**, *136*, 4369.

(5) Platero-Prats, A. E.; de la Peña-ÓShea, V. A.; Snejko, N.; Monge, A.; Gutiérrez-Puebla, E. *Chem.—Eur. J.* **2010**, *16*, 11632−11640.

(6) Horcajada, P.; Gref, R.; Baati, T.; Allan, P. K.; Maurin, G.; Couvreur, P.; Férey, G.; Morris, R. E.; Serre, C. *Chem. Rev.* **2012**, *112*, 1232−1268.

(7) Corma, A.; García, H.; Llabrés i Xamena, F. X. *Chem. Rev.* **2010**, *110*, 4606−4655.

(8) Ma, L.; Abney, C.; Lin, W. *Chem. Soc. Rev.* **2009**, *38*, 1248−1256.

(9) (a) Allendorf, M. D.; Bauer, C. A.; Bhaktaa, R. K.; Houk, R. J. T. *Chem. Soc. Rev.* **2009**, *38*, 1330−1352. (b) Monge, A.; Gándara, F.; Gutiérrez-Puebla, E.; Snejko, N. *CrystEngComm* **2011**, *13*, 5031−5044. (c) D'Vries, R. F.; Alvarez-Garcia, S.; Snejko, N.; Bausa, L. E.; Gutierrez-Puebla, E.; de Andres, A.; Monge, M. A. *J. Mater. Chem. C* **2013**, *1*, 6316.

(10) (a) Miller, J. S.; Gatteschi, D. *Chem. Soc. Rev.* **2011**, *40*, 3065. (b) Coronado, E.; Dunbar, K. R. *Inorg. Chem.* **2009**, *48*, 3293.

(11) Ramesh, R.; Spaldin, N. A. *Nat. Mater.* **2007**, *6*, 21−29.

(12) (a) Gavrilenko, K. S.; Punin, S. V.; Cador, O.; Golhen, S.; Ouahab, L.; Pavlishchuk, V. V. *J. Am. Chem. Soc.* **2005**, *127*, 12246. (b) Park, G.; Kim, H.; Lee, G. H.; Park, S.-K.; Kim, K. *Bull. Korean Chem. Soc.* **2006**, *27*, 443. (c) Yao, M.-X.; Zeng, M.-H.; Zou, H.-H.; Zhou, Y.-L.; Liang, H. *Dalton Trans.* **2008**, 2428. (d) Luo, J.; Zhao, Y.; Xu, H.; Kinnibrugh, T. L.; Yang, D.; Timofeeva, T. V.; Daemen, L. L.; Zhang, J.; Bao, W.; Thompson, J. D.; Currier, R. P. *Inorg. Chem.* **2007**, *46*, 9021.

(13) Kurmoo, M. *Chem. Soc. Rev.* **2009**, *38*, 1353 and references therein.

(14) Bernini, M. C.; Platero-Prats, A. E.; Snejko, N.; Gutierrez-Puebla, E.; Labrador, A.; Saez-Puche, R.; Romero de Paz, J.; Monge, M. A. *CrystEngComm* **2012**, *14*, 5493−5504.

(15) *Siemens SMART system*, with SAINT data collection and procedure software; Siemens Analytical X-ray Instruments, Inc.: Madison, WI, 1995.

(16) *Siemens SHELXTL*, version 5.0, Siemens Analytical X-ray Instruments Inc.: Madison, WI, 1995.

(17) Spek, A. L. *Acta Crystallogr., Sect. A* **1990**, *46*, C34.

(18) Bain, G. A.; Berry, J. F. *J. Chem. Educ.* **2008**, *85*, 532−536.

(19) (a) Kirillov, A. M.; Kopylovich, M. N.; Kirillova, M. V.; Haukka, M.; Guedes da Silva, M. F. C.; Pombeiro, A. J. L. *Angew. Chem., Int. Ed.* **2005**, *44*, 4345−4349. (b) Langley, S. K.; Berry, K. J.; Moubaraki, B.; Murray, K. S. *Dalton Trans.* **2009**, 973−982. (c) Buvaylo, E. A.; Kokozay, V. N.; Vassilyeva, O. Y.; Skelton, B. W.; Eremenko, I. L.; Jezierska, J.; Ozarowski, A. *Inorg. Chem.* **2009**, *48*, 11092−11097.

(20) Li, C.-P.; Du, M. *Chem. Commun.* **2011**, *47*, 5958−5972.

(21) Bernini, M. C.; Snejko, N.; Puebla, E. G.; Brusau, E. V.; Narda, G. E.; Monge, M. A. *Inorg. Chem.* **2011**, *50*, 5958.

(22) (a) Monge, A.; Snejko, N.; Gutiérrez-Puebla, E.; Medina, M.; Cascales, C.; Ruiz-Valero, C.; Iglesias, M.; Gómez-Lor, B. *Chem. Commun.* **2005**, 1291. (b) Gándara, F.; Medina, M.; Snejko, N.; Gutiérrez-Puebla, E.; Proserpio, D. M.; Monge, M. A. *CrystEngComm* **2010**, *12*, 711. (c) Gándara, F.; de Andrés, A.; Gómez-Lor, B.; Gutiérrez-Puebla, E.; Iglesias, M.; Monge, M. A.; Proserpio, D. M.; Snejko, N. *Cryst. Growth Des.* **2008**, *8*, 378. (d) Gándara, F.; de la Peña-O'Shea, V. A.; Illas, F.; Snejko, N.; Proserpio, D. M.; Gutiérrez-Puebla, E.; Monge, M. A. *Inorg. Chem.* **2009**, *48*, 4707.

(23) Wang, X.; Liu, L.; Conato, M.; Jacobson, A. J. *Cryst. Growth Des.* **2011**, *11*, 2257−2263.

(24) *Materials Studio*, v6.1; Accelrys Software Inc.: San Diego, CA

12894

dx.doi.org/10.1021/ic501898x | *Inorg. Chem.* 2014, 53, 12885−12895

(25) Hajjar, R.; Volkringer, C.; Loiseau, T.; Guillou, N.; Marrot, J.; Ferey, G.; Margiolaki, I.; Fink, G.; Morais, C.; Taulelle, F. *Chem. Mater.* **2011**, *23* (1), 39−47.

(26) Blatov, V. A.; Shevchenko, A. P.; Proserpio, D. M. *Cryst. Growth Des.* **2014**, *14*, 3576−3586.

(27) (a) Li, L.; Ma, J.; Chen, T.; Sun, Z.; Wang, S.; Luo, J.; Hong, M. *Inorg. Chem.* **2012**, *51*, 2438−2442. (b) Liu, Q.-Y.; Wang, Y.-L.; Shan, Z.-M.; Cao, R.; Jiang, Y.-L.; Wang, Z.-J.; Yang, E.-L. *Inorg. Chem.* **2010**, *49*, 8191−8193. (c) Cao, L.-H.; Xu, Q.-Q.; Zang, S.-Q.; Hou, H.-W.; Mak, T C. W *Cryst. Growth Des.* **2013**, *13*, 1812−1814.

(28) Mabbs, F. E.; Machin, D. J. *Magnetism and Transition Metal Complexes;* Dover Publications: Toronto, CA, 2008.

(29) Saouma, C. T.; Peters, J.C. *Coord. Chem. Rev.* **2011**, *255*, 920−937.

(30) Bersuker, I. B. *Chem. Rev.* **2013**, *113*, 1351−1390.

(31) Nishida, Y.; Kida, S. *J. Chem. Soc., Dalton Trans.* **1986**, 2633−2640.

(32) Goodenough, J. B. *Magnetism and the Chemical Bond;* John Wiley and Sons: New York, 1963.

(33) Kanamori, J. *J. Phys. Chem. Solids* **1959**, *10*, 87−98.

(34) Popov, O.; Mikhov, M. *J. Magn. Magn. Mater.* **1988**, *75*, 135−140.

(35) Oka, Y.; Inoue, K. *Chem. Lett.* **2004**, *33*, 402−403.

(36) Dwight, K.; Menyuk, N. *Phys. Rev.* **1960**, *119*, 1470−1479.